TECHNICAL INNOVATION

CrossMark
click for updates

Recreating mineralogical petrographic heterogeneity within microfluidic chips: assembly, examples, and applications†

Stephen A. Bowden,‡[a] Yukie Tanino,‡*[b] Blessing Akamairo[a] and Magali Christensen[b]

To date, the visualisation of flow through porous media assembled in microfluidic chips was confined to mineralogically homogenous systems. Here we present a key evolution in the method that permits the investigation of mineralogically realistic rock analogues.

Micromodels have been used for decades to visualize multi-phase flow through porous media by earth scientists, groundwater hydrologists, and petroleum engineers interested in the physical processes that govern the flow of immiscible fluids through soil, sediment, and rock. The earliest micromodels were of uniform pore geometry etched in resin or glass or silicon.[1] In the past decade, researchers have begun creating micromodels with more complex pore geometry by transferring *via* photo lithography and then etching thin section[2–5] or X-ray microcomputed tomography[6,7] images of real rock into a single acid-etchable material such as silicon, quartz, glass, or calcite.

These models allow dynamic imaging of pore-scale processes, but because they are etched from a single material they do not capture the scope of the variation seen in the mineralogical composition of rock (petrographic variation), nor the corresponding variations in rock/fluid chemical interaction, grain texture, and grain size and shape. In rock, such variations occur at all scales, from nm (sub-pore scale) to km. For example, random variations in the hydrophilicity and elasticity over length scales as small as 50 nm have been reported in Danish North Sea chalk.[8] Rocks often display mm-scale variations in mineralogy which result from the sequential deposition of laminae that possess distinctive mineralogy. For different types of sedimentary rock (different lithologies), variation at the mm-scale may be slow and gradational (*e.g.*, from the base to the top of a lamination) or clearly defined and sharp depending on the depositional process. Accordingly, such variations are fundamental in classifying petrographic features as important as mineralogy. Furthermore, because sedimentary successions can often be described in terms of facies models – conceptual models that explain the occurrence of different types of rock in both time and space[9] – hydraulic properties of much larger sedimentary units can be extrapolated from smaller observations.[10]

Rock/fluid interaction and grain size, shape, and texture – and their spatial variation – determine the distribution of fluids over a wide range of scales and consequently their displacement. Sub-pore scale heterogeneity in hydrophilicity due to differential exposure to non-aqueous phase liquids (NAPL), commonly referred to as mixed wettability, is associated with dramatically protracted recovery of non-aqueous phases from oil reservoirs and NAPL-contaminated aquifers.[11–13] Similarly, pore size and topology largely determine permeability, and their variation at the reservoir scale give rise to bypassing and poor oil recovery.[14] Despite the long history of microfluidic studies, previous work has not addressed the consequences of the varied surface properties of the different mineral components of sedimentary rocks at the pore scale and lamina scale. This is remarkable when mineralogical composition is an inherent and fundamental rock property used for classification (*e.g.*, QFL-scheme of siliciclastic rocks).[15] One reason for this may be the previous monolithic composition of micromodels.

To explore the impact of lamina-scale heterogeneities in mineralogy on two-phase flow through porous media under conditions representative of the subsurface, we developed a technique for rapid, low-cost assembly of single-use "micromodels" that recreate mineralogical heterogeneities at the $O(100)$ μm to $O(1)$ mm scale. This paper reports oil recovery measurements on uniform and layered micromodels which, combined, demonstrate the complex flow behaviour that emerges in the presence of structured variations.

Our micromodels are unconsolidated, quasi-2.5-dimensional beds of mineral grains packed into custom-

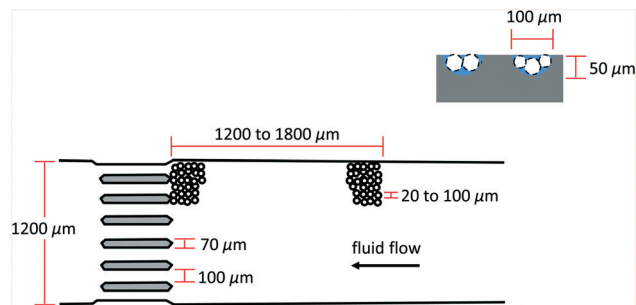[a] *Dept. Geology and Petroleum Geology, University of Aberdeen, Aberdeen AB24 3UE, UK*
[b] *School of Engineering, University of Aberdeen, Aberdeen AB24 3UE, UK. E-mail: ytanino@abdn.ac.uk*

Fig. 1 Plan view of the microfluidic channel in which the packed bed is assembled. Fluids are dispensed from two ports on the right 14 or 18 mm upstream of the gap filter, and expelled from a single port on the left (not shown).

made 1200 μm-wide and 50 μm-deep channels etched in soda lime glass (Fig. 1, Dolomite Centre Ltd.).

Grains. For silica, commercially available soda lime glass spheres (White House Scientific, UK) are used.[16] Suitable products are not commercially available for other minerals and, accordingly, we prepare these grains by crushing rock (*e.g.*, marble[17]) or single crystals (*e.g.*, orthoclase). Further details are provided in ESI,† along with the characterisation of materials used in the experiments presented below. Two key advantages of using crushed rock are the partial conservation of surface roughness and grooves (*e.g.*, Fig. S1 and S2†) and intra-grain heterogeneities in mineral composition. Both influence *in situ*, pore-scale contact angles[18–20] and hence the distribution and displacement of fluids within a porous medium. In addition, roughness and grooves on grain surfaces permit the wetting phase to remain connected even to low saturations and promote capillary trapping of the non-wetting phase by snap-off, increasing residual oil saturation in water-wet porous media.[21–23]

Assembly of layered beds. Packed beds are assembled by wet-packing, *i.e.*, by flushing suspensions of grains. A gap filter comprised of 100 μm-diameter, semi-circular channels retains the grains in the channel (Fig. 1). Micron- to mm-scale structures are assembled by sequentially injecting suspensions of grains of different mineralogy until a pack or a lamina of the desired length assembles behind the gap filter (Fig. 2). The carrier phase is chosen to be non-aqueous and chemically inert with respect to the mineral phase being used to suppress cohesion; *n*-hexane was used in all experiments presented below. The concentration of grains in the suspension is kept low (1 : 7 to 1 : 9 v/v unconsolidated particles to liquid phase) to avoid blockages in ancillary tubing.

Fig. 3 and 4 illustrate the application of this technique to recreating a finely laminated siltstone from the top of the Poll a'Mahuillt member of the Stoer Group in NW Scotland.[24] The siltstone comprises alternating laminae of fine grained silica and coarser grained orthoclase feldspar and quartz. The packed beds assembled within a microfluidic chip similarly comprise sub-mm laminae of orthoclase and silica (*e.g.*, Fig. 4b). The key difference between the two packs is the thickness of the orthoclase lamina, which is 890 μm (or 14
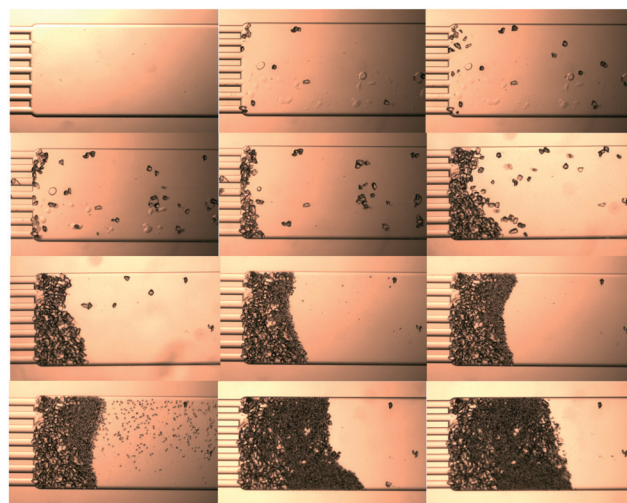
Fig. 2 Assembly of a laminated packed bed. Grains are moved using gently pulsed flow (pulses are created by tapping the syringe plunger). Resolution is 2.4 μm per pixel.

grain diameters, *cf.* Table S3†)-thick in the first analogue (Fig. 3) and 200 μm (3 grain diameters)-thick in the second (Fig. 4).

Displacement experiments. The experimental procedure employed to study the flow of immiscible fluids in these beds closely follows that presented previously for uniform beds.[16,17] In short: syringe pumps are used to dispense fluids into the packed bed, and a high-speed 24 bit colour camera coupled to an optical microscope is used to capture the packed bed in a sequence of still images. The acquired
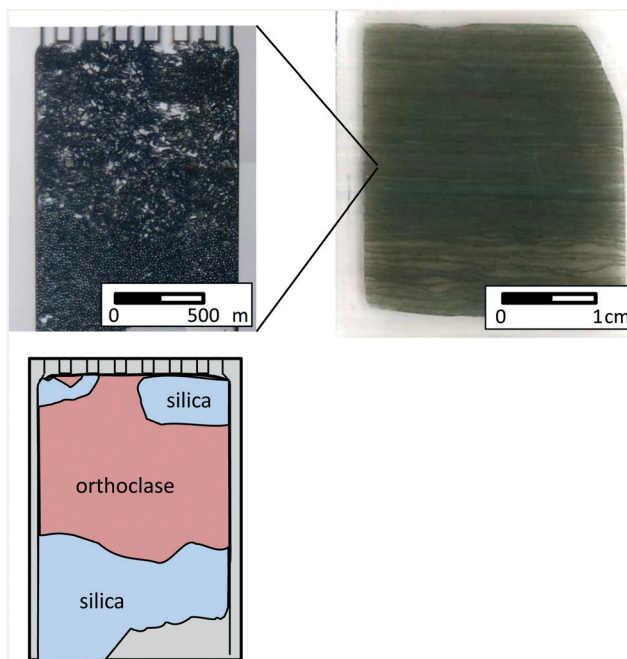
Fig. 3 A feldspathic siltstone from Stoer Group outcrops, NW Scotland: thin section (right) and its microfluidic analogue (left) and corresponding mineralogy (bottom).
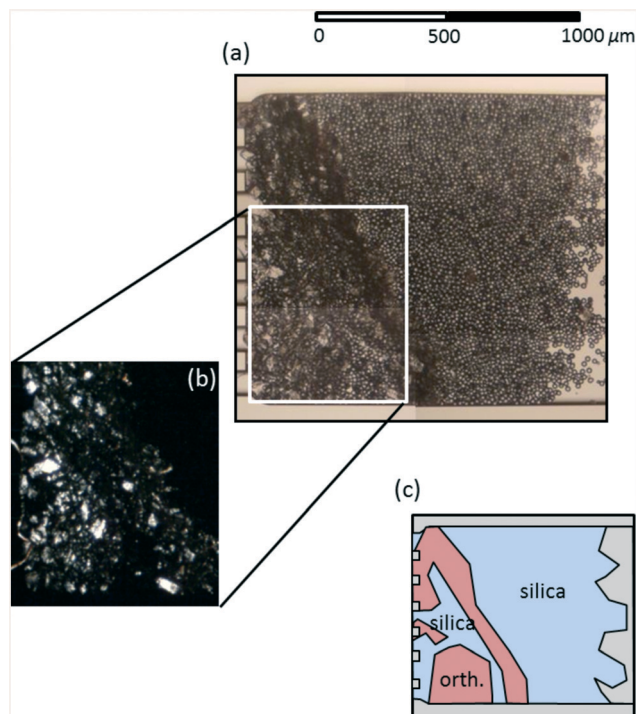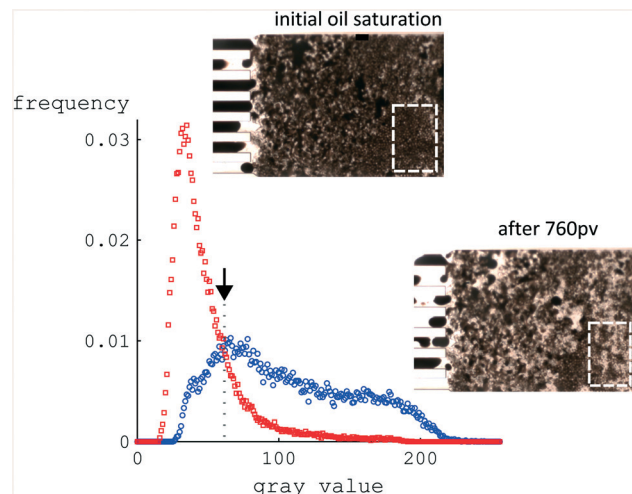
Fig. 4 A second siltstone analogue: (a) photomosaic and (c) an interpretation of its mineralogy; (b) view of the feldspathic zone in cross polarised light (commonly used in petrography to identify different mineral components in rock and sediment) in which orthoclase exhibits bright birefringence colours but silica, which is glass-like, does not.

Fig. 5 Histogram of gray values at the onset of waterflood (red square) and towards the end of the experiment (blue circle) in a region of interest; the dashed box demarcates the analyzed region in the corresponding raw images. Vertical arrow indicates the intersection of the two frequency distributions. Packed bed is the same as that shown in Fig. 3.

images are converted to gray scale and segmented to determine the distribution of the fluids within the packed bed at a given instance.

The segmentation threshold is determined from the gray value histograms of two images during the waterflood: one at the onset of waterflood (*e.g.*, red squares, Fig. 5) and one towards the end of the waterflood (blue circles). As waterflood progresses and water content in the packed bed increases, the frequencies of lower gray values (darker pixels) decrease and those of higher gray values (brighter pixels) increase. The intersection between the two distributions, *i.e.*, the lowest gray value whose frequency increases as waterflood progresses, is taken as the threshold (arrow, Fig. 5). Water saturation at a given instance is then given by the fraction of pixels within the region of interest with gray values larger than this threshold. Because refractive properties vary between different minerals (*e.g.*, calcite generates double refractions) and with crystallographic orientation, a segmentation threshold is determined for each lamina separately.

The displacement sequence itself is designed to mimic that in the application of interest. The packed bed is first cleaned with a sequence of solvents that finishes with a solvent that can be easily solubilised by the primary phase. For model oil reservoirs, the primary phase is a brine representative of the water present in the reservoir prior to the invasion of oil. Next, a volume of the primary phase equivalent to 100

times the pore volume (pv) of the packed bed is flushed through the chip. The test oil is then injected into the packed bed to mimic buoyancy-driven oil invasion; a high flow rate is used to create back pressure to facilitate the establishment of a uniform oil saturation. The chip may then be left at elevated temperature ('aged') so that adsorption and other surface chemistry processes can reach equilibrium. Finally, an aqueous phase is dispensed to displace the oil in the packed bed to mimic waterflood oil recovery.

To demonstrate the impact of lamina-scale structure on oil distribution and recovery, waterflood experiments were undertaken on four packed beds: a uniform silica bed, a uniform orthoclase bed, and the two laminated siltstone analogues in Fig. 3 and 4, respectively (Table 1). The test oil was a topped (light components removed) medium crude oil. The aqueous phase was either 5.0 wt% NaCl, 1.0 wt% KCl in deionised water (hereafter referred to as synthetic brine) or coastal seawater; further details can be found in ESI.† The packed beds were aged at 45 °C for 40 minutes at initial oil saturation, after which they were allowed to cool to ambient temperature before water was injected at constant flow rate.§

Fig. 6 (top row) presents images captured at different stages of the waterflood for the two heterogeneous beds: (i) prior to water injection, (ii) after the injection of a moderate volume analogous to a mature oil field (1–2 pv), and (iii) after the injection of a greater pore volume (40 pv).

The contrast in flow behaviour between the two laminated beds is readily seen. Oil was displaced uniformly from the entire packed bed when the orthoclase-rich lamina was

---

§ A higher flow rate was used in the heterogeneous packed beds than in the uniform, single mineral beds (Table 1). However, we previously showed using the same oil and seawater that water saturation is independent of flow rate for Darcy velocities between $8 < U_w < 1760$ μm s^{-1} after 10 pv.[17]

Table 1 Experimental conditions. Only the lengths of the dominant silica and orthoclase-rich laminae are reported below for the heterogeneous packs (*cf.* Fig. 3 and 4). The aqueous phase was synthetic brine for the uniform silica bed, and seawater for all others

Pack mineralogy	U_w (µm s^{-1})	pv (nL)	Resolution (µm pix^{-1})	
Silica, 1.7 mm	350	39	2.5	
Orthoclase, 1.3 mm	340	29	3.0	
600 µm silica, 890 µm orthoclase	850	34	2.5	Fig. 3
770 µm, 200 µm orthoclase	850	29	3.0	Fig. 4
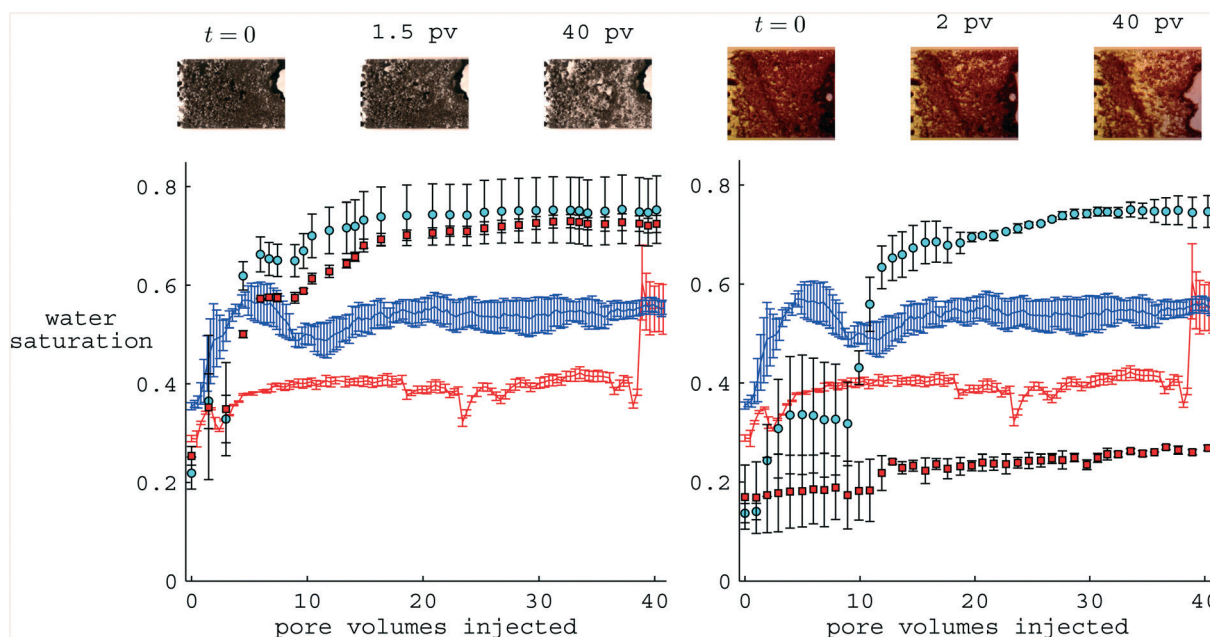
Fig. 6 Selected raw images (top row) and lamina-averaged water saturation (bottom row) in the upstream silica-rich region (cyan solid circle) and the subsequent orthoclase-rich (red solid square) region during a waterflood experiment on the packed beds shown in Fig. 3 (left) and 4 (right). Superposed are mean water saturations in uniform beds of orthoclase (red dotted line) and silica (blue solid line). Vertical bars depict the difference between two regions (typically the two half-widths of the channel) within the lamina of interest. Flow is right to left in the images.

relatively thick (Fig. 6, left). In contrast, oil was preferentially recovered from the silica-rich regions of the packed bed when the orthoclase-rich region was thin. Indeed, the water saturation within the orthoclase-rich region increased only marginally to 25% after 30 pv of water injection (bottom row, right).
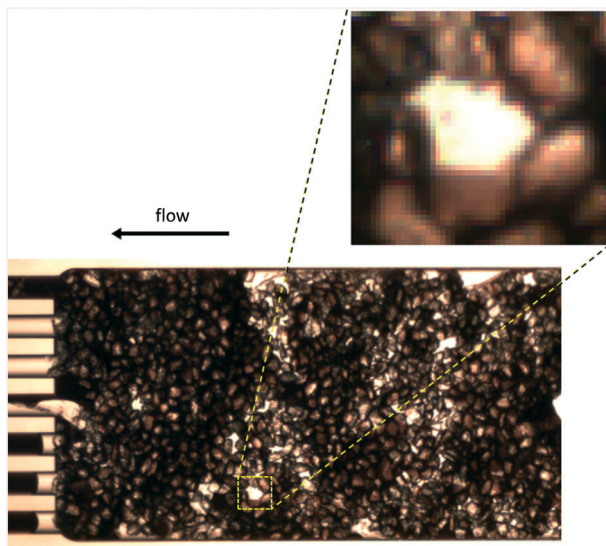
The observed differences may be attributed to differences in grain roughness and lamina thickness. Silica grains are both smooth and of uniform grain size (Fig. S3†), so water tends to invade the pores uniformly, displacing oil from them. In contrast, the grooves on the rough orthoclase surfaces (Fig. S1†) provide a pathway for water to flow through the orthoclase-rich lamina without displacing the oil in the bulk of the pore space. However, the permeability of these thin pathways is very low, so if the orthoclase-rich lamina is sufficiently long, the pressure gradient required to accommodate the imposed injection rate will drive the water into the centers of the pores, thereby displacing the oil in them and giving rise to a more efficient recovery.

The lamina-averaged water saturation (Fig. 6, bottom row) indicates that oil recovery from the main silica zone in the two laminated beds (cyan circles) were more efficient, with water saturation reaching 75% after 30 pv in both cases, than

that from the uniform bed (blue solid line). This discrepancy highlights the influence of the orthoclase lamina on the upstream silica layer, and indicates that the impact of mineralogical discontinuities can extend upstream. This may have important implications not only for laminated rock but for other systems with capillary discontinuities, *e.g.*, fractured reservoirs.

A further strength of the method is that the distribution of the fluids can be visualized at the pore scale and sub-pore scale. To illustrate, Fig. 7 presents a uniform bed of crushed marble,† our microfluidic analogue of carbonate rock, at the later stages of a waterflood. It can be seen that water has displaced the oil completely from the center of the large pore captured in the inset, while a small volume of oil remains as a thin film along the surface of the grains surrounding it. This observed pore-scale distribution is direct evidence that the grains have been rendered oil-wet from exposure to the oil. This conclusion is corroborated by pore-scale observations: the water preferentially invaded the largest pores first. The largest pores are associated with the lowest capillary entry pressure to the non-wetting phase, so this invasion pattern indicates that oil has become the wetting phase. Also,

Fig. 7 A microfluidic analogue of carbonate rock after 52 pv of water injection; pore volume was 83 nL. Inset captures a 180×156 μm region. The flood water was synthetic brine; $U_w = 28$ μm s^{-1}. The chip was aged at initial oil saturation for 120 minutes at 45 °C. Resolution is 3.0 μm per pixel.

References

1   R. Lenormand, C. Zarcone and A. Sarr, *J. Fluid Mech.*, 1983, **135**, 337–353.
2   E. R. Rangel-German and A. R. Kovscek, *Water Resour. Res.*, 2006, **42**, W03401.
3   W. Song, T. W. de Haas, H. Fadaei and D. Sinton, *Lab Chip*, 2014, **14**, 4382–4390.
4   J. Wan, T. K. Tokunaga, C.-F. Tsang and G. S. Bodvarsson, *Water Resour. Res.*, 1996, **32**, 1955–1964.
5   C. A. Conn, K. Ma, G. J. Hirasaki and S. L. Biswal, *Lab Chip*, 2014, **14**, 3968–3977.
6   M. L. Porter, J. Jimenez-Martinez, R. Martinez, Q. McCulloch, J. W. Carey and H. S. Viswanathan, *Lab Chip*, 2015, **15**, 4044–4053.
7   A. Gerami, P. Mostaghimi, R. T. Armstrong, A. Zamani and M. E. Warkiani, *Int. J. Coal Geol.*, 2016, **159**, 183–193.
8   T. Hassenkam, L. L. Skovbjerg and S. L. S. Stipp, *Proc. Natl. Acad. Sci. U. S. A.*, 2009, **106**, 6071–6076.
9   R. G. Walker and N. P. James, *Facies Models: Response to Sea Level Change*, Geological Association of Canada, 1992.
10 J. C. Van Wagoner, R. M. Mitchum, K. M. Campion and V. D. Rahmanian, *Siliciclastic Sequence Stratigraphy in Well Logs, Cores, and Outcrops: Concepts for High-Resolution Correlation of Time and Facies*, American Association of Petroleum Geologists Methods in Exploration 7, 1990.
11 Y. Tanino and M. J. Blunt, *Water Resour. Res.*, 2013, **49**, 4311–4319.
12 R. A. Salathiel, *Soc. Pet. Eng. J.*, 1973, **25**, 1216–1224.
13 A. R. Kovscek, H. Wong and C. J. Radke, *AIChE J.*, 1993, **39**, 1072–1085.
14 A. Muggeridge, A. Cockin, K. Webb, H. Frampton, I. Collins, T. Moulds and P. Salino, *Philos. Trans. R. Soc., A*, 2014, **372**, 20120320.
15 L. J. Suttner, A. Basu and G. H. Mack, *J. Sediment. Res.*, 1981, **51**, 1235–1246.
16 S. A. Bowden, J. M. Cooper, F. Greub, D. Tambo and A. Hurst, *Lab Chip*, 2010, **10**, 819–823.
17 Y. Tanino, B. Akamairo, M. Christensen and S. A. Bowden, *Proc., International Symposium of the Society of Core Analysts, St. John's Newfoundland and Labrador*, Canada, 2015.
18 N. R. Morrow, *J. Can. Pet. Technol.*, 1975, **14**, 42–53.
19 L. E. Treiber, D. L. Archer and W. W. Owens, *Soc. Pet. Eng. J.*, 1972, **12**, 531–540.
20 J. Drelich, J. D. Miller and R. J. Good, *J. Colloid Interface Sci.*, 1996, **179**, 37–50.
21 Q. Meng, H. Liu, J. Wang and H. Zhang, *Energy Fuels*, 2016, **30**, 835–843.
22 F. A. L. Dullien, C. Zarcone, I. F. Macdonald, A. Collins and R. D. E. Bochard, *J. Colloid Interface Sci.*, 1989, **127**, 362–372.
23 G. N. Constantinides and A. C. Payatakes, *Transp. Porous Media*, 2000, **38**, 291–317.
24 J. Parnell, A. J. Boyce, D. Mark, S. A. Bowden and S. Spinks, *Nature*, 2010, **468**, 290–293.

much of the oil remains connected even after tens of pv of water injection which, as discussed earlier, is a salient feature of mixed wet systems.

Microscaled porous media experiments permit a wide range of geological variables to be investigated and mineralogical composition is clearly at the forefront of under-investigated parameters. The experiments presented here illustrate that measurable differences in recovery result from not only global differences in wetting preference, but also from petrographic variables and factors such as the type of minerals involved and their architecture (*e.g.*, lamination style). These findings highlight the importance of considering mineralogical heterogeneity when using microfluidic experiments to evaluate oil recovery. Packed beds assembled from key rock forming minerals are a novel tool for this purpose.

Acknowledgements